



## Ground-state phase diagram of the one-dimensional $t$ - $J_s$ - $J_\tau$ model at quarter filling

Yuya Kurebayashi <sup>1,\*</sup>, Hiroki Oshiyama <sup>2</sup>, and Naokazu Shibata <sup>1</sup>

<sup>1</sup>*Department of Physics, Tohoku University, Sendai 980-8578, Japan*

<sup>2</sup>*Graduate School of Information Science, Tohoku University, Sendai 980-8579, Japan*

 (Received 7 December 2020; revised 19 March 2021; accepted 2 April 2021; published 14 April 2021)

We study the ground state of the one-dimensional “ $t$ - $J_s$ - $J_\tau$  model,” which is a variant of the  $t$ - $J$  model with an additional channel degree of freedom. The model is not only a generalization of the  $t$ - $J$  model but also an effective model of the two-channel Kondo lattice model in the strong-coupling region. The low-energy excitations and correlation functions are systematically calculated by the density matrix renormalization group method, and the ground-state phase diagram at quarter filling consisting of a Tomonaga-Luttinger liquid, spin-gap state, channel-gap state, insulator, and phase separation is determined. We find that weak channel fluctuations stabilize the spin-gap state, while strong channel fluctuations lead to the transition to the insulator.

DOI: [10.1103/PhysRevB.103.165115](https://doi.org/10.1103/PhysRevB.103.165115)

### I. INTRODUCTION

Quantum fluctuations are important features of microscopic systems, which give rise to plenty of interesting phenomena. In condensed-matter physics, spin fluctuations play an important role in realizing various quantum states, such as spin liquids and superconductivity. One of the minimal theoretical models containing both spin and charge degrees of freedom is the  $t$ - $J$  model. The model was originally proposed to describe high- $T_c$  superconductivity [1], and its one-dimensional model has been studied to understand the fundamental properties of strongly correlated systems. Although this model contains only the kinetic energy term and the exchange energy term, various quantum states including a spin-gap state are realized [2], and it is interesting to investigate whether new quantum states appear when we include additional interactions existing in more realistic systems. One simple extension is the inclusion of repulsive interaction  $V$  between the neighboring electrons. It has been reported that the repulsive interaction  $V$  stabilizes the spin-gap phase at quarter filling [3], but other new states have not yet been obtained. Another approach to extend the  $t$ - $J$  model is to add new degrees of freedom of electrons.

Praseodymium contained in cage-shaped composites, such as PrTi<sub>2</sub>Al<sub>20</sub>, has a non-Kramers doublet as the crystal-field ground state [4,5]. The theoretical model of such materials is the two-channel Kondo lattice model (TCKLM) [6,7], which has multiple degrees of freedom associated with the non-Kramers doublets. As one of the simplest models of interacting electron systems consisting of multiple degrees of freedom, we propose the “ $t$ - $J_s$ - $J_\tau$  model,” which is not only an extension of the  $t$ - $J$  model but also an effective model of the TCKLM in the strong-coupling region.

In this paper, we study the ground-state properties of the model by the density matrix renormalization group (DMRG)

method and investigate the effect of the channel degree of freedom on the ground state. The obtained results show that the spin-gap state is stabilized by weak channel fluctuations, while strong channel fluctuations lead to the transition to the insulator.

### II. MODEL

The model we study here is the following  $t$ - $J_s$ - $J_\tau$  model:

$$H_{tJJ} = -t \sum_{i\sigma} (a_{i\sigma}^\dagger b_{i\alpha} b_{i+1,\alpha}^\dagger a_{i+1,\sigma} + \text{H.c.}) + J_s \sum_i \mathbf{S}_i \cdot \mathbf{S}_{i+1} + J_\tau \sum_i \boldsymbol{\tau}_i \cdot \boldsymbol{\tau}_{i+1} + V \sum_i n_i n_{i+1}, \quad (1)$$

where  $a_{i\sigma}^\dagger$  and  $b_{i\alpha}^\dagger$  are the creation operators of particles and “holes” at the  $i$ th site with spin  $\sigma$  and channel  $\alpha$ , respectively, and the empty and double occupancies of  $a_{i\sigma}^\dagger$  and  $b_{i\alpha}^\dagger$  are inhibited:

$$\sum_{\sigma} a_{i\sigma}^\dagger a_{i\sigma} + \sum_{\alpha} b_{i\alpha}^\dagger b_{i\alpha} = n_i + \sum_{\alpha} b_{i\alpha}^\dagger b_{i\alpha} = 1, \quad (2)$$

where  $n_i = \sum_{\sigma} a_{i\sigma}^\dagger a_{i\sigma}$  is the number operator of the particles. The spin and channel-pseudospin operators are defined as  $\mathbf{S}_i = \frac{1}{2} \sum_{\sigma\sigma'} a_{i\sigma}^\dagger \boldsymbol{\sigma}_{\sigma\sigma'} a_{i\sigma'}$  and  $\boldsymbol{\tau}_i = \frac{1}{2} \sum_{\alpha\alpha'} b_{i\alpha}^\dagger \boldsymbol{\sigma}_{\alpha\alpha'} b_{i\alpha'}$ , respectively.

This model is not only a generalization of the extended  $t$ - $J$  model but also derived from the TCKLM

$$H_{\text{TCKLM}} = -\tilde{t} \sum_{i\sigma\alpha} (c_{i\alpha\sigma}^\dagger c_{i+1,\alpha\sigma} + \text{H.c.}) + \frac{J}{2} \sum_{i\alpha\sigma\sigma'} \tilde{\mathbf{S}}_i \cdot (c_{i\alpha\sigma}^\dagger \boldsymbol{\sigma}_{\sigma\sigma'} c_{i\alpha\sigma'}), \quad (3)$$

$$\tilde{\mathbf{S}}_i = \frac{1}{2} \sum_{\sigma\sigma'} f_{i\sigma}^\dagger \boldsymbol{\sigma}_{\sigma\sigma'} f_{i\sigma'}, \quad (4)$$

\*kurebayashi@cmpt.phys.tohoku.ac.jp

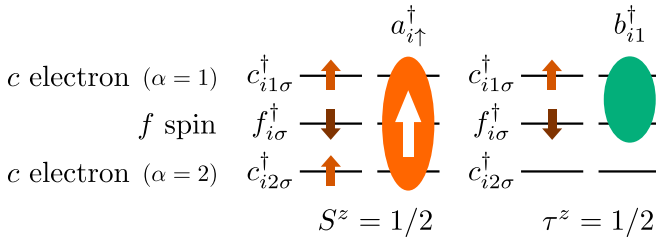


FIG. 1. Schematic representations of the composite particles  $a_{i\uparrow}^\dagger$  and  $b_{i\uparrow}^\dagger$  in the TCKLM.

as follows: assuming that the number of conduction electrons per local spins  $n_c$  satisfies  $1 \leq n_c \leq 2$ , the effective Hamiltonian in the strong-coupling region is given by the second-order perturbation of  $1/J$  from the limit  $J/\tilde{t} = \infty$ . In this case,  $a^\dagger$  and  $b^\dagger$  are the composite particles defined as  $a_{i\sigma}^\dagger = \frac{1}{\sqrt{6}}(2c_{i1\sigma}^\dagger c_{i2\sigma}^\dagger f_{i\bar{\sigma}}^\dagger - c_{i1\sigma}^\dagger c_{i2\bar{\sigma}}^\dagger f_{i\sigma}^\dagger - c_{i1\bar{\sigma}}^\dagger c_{i2\sigma}^\dagger f_{i\sigma}^\dagger)$  and  $b_{i\sigma}^\dagger = \frac{1}{\sqrt{2}}(c_{i\alpha\uparrow}^\dagger f_{i\downarrow}^\dagger - c_{i\alpha\downarrow}^\dagger f_{i\uparrow}^\dagger)$ , respectively, as schematically represented in Fig. 1. The transfer integral  $t$  in Eq. (1) is given as  $t = 3\tilde{t}/4$ , and the effective interactions are

$$J_s = \frac{1504t^2}{135J}, \quad J_\tau = \frac{64t^2}{9J}, \quad \frac{J_\tau}{J_s} \approx 0.64. \quad (5)$$

The interactions  $J_s$  and  $J_\tau$  are the two largest terms obtained by the perturbation expansion, and the other ones, including next-nearest hopping, are ignored. The neglected long-range interactions are expected to suppress the phase separation caused by the above two interactions. Instead of treating all such terms explicitly, we consider the repulsion term  $V$  to suppress the phase separation. Note that when  $n_c = 1$ , which corresponds to the absence of  $a^\dagger$  particles ( $n = 0$ ), the model is reduced to the Heisenberg model of the channel degree of freedom [7].

In this study, we analyze the ground state of the Hamiltonian of Eq. (1) with an equal number of particles and holes at  $n = 1/2$  (quarter filling,  $k_F = \pi/4$ ). This filling corresponds to  $n_c = 3/2$  in the TCKLM. Throughout this paper, we fix the nearest-neighbor interaction  $V$  as  $V/t = 0.8$  and take the transfer integral  $t$  as the unit of energy.

### III. METHOD

We use the DMRG method [8,9] to analyze the ground states of the Hamiltonian of Eq. (1). In this method, the accuracy of the ground-state wave function is systematically controlled by the number of remaining states  $m$ . We increase  $m$  up to 400 to see the convergence of the results, where the truncation error is less than  $10^{-5}$ . The system size is in the range of 128–192.

To suppresses the finite-size effect caused by the open boundary conditions used in the DMRG calculation, we apply the sine square deformation (SSD) [10] to the Hamiltonian. Since the SSD reproduces the bulk response to an external field [11], we use this property to obtain the excitation gap of the infinite system.

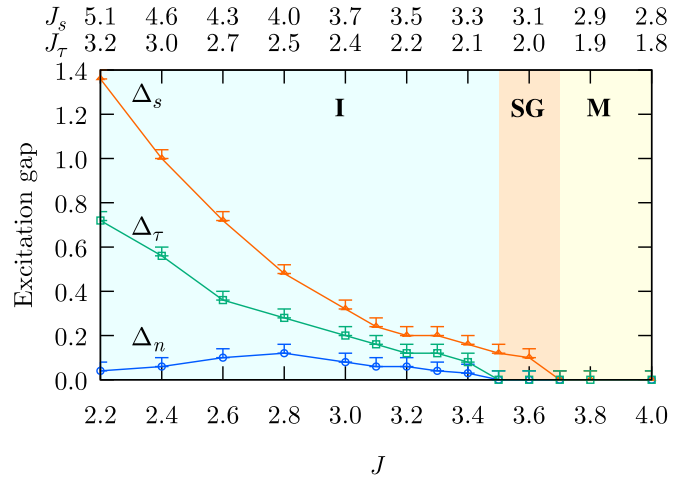


FIG. 2. Excitation gaps for the charge  $\Delta_n$ , spin  $\Delta_s$ , and channel  $\Delta_\tau$  degrees of freedom. The upper axes represent the effective interactions defined in Eqs. (5). The error bars are introduced by the discrete parameter settings used in the SSD method [11].

### IV. RESULT

We first study the elementary excitations of the model to clarify how the interactions modify the low-energy properties of the system. We calculate the excitation gap for the charge ( $\Delta_n$ ), spin ( $\Delta_s$ ), and channel ( $\Delta_\tau$ ) degrees of freedom in the parameter space of  $J_s$ - $J_\tau$ . Figure 2 shows the excitation gaps obtained along the line defined by Eq. (5). With decreasing the parameter  $J$  of the TCKLM (with increasing  $J_s$  and  $J_\tau$  of the  $t$ - $J_s$ - $J_\tau$  model), the spin excitation gap first opens, and then, the charge and channel gaps open.

These successive transitions show the presence of the spin-gap phase. To further confirm the spin-gap phase, we systematically calculate the excitation gaps for various  $J_s$  and  $J_\tau$  and determine the ground-state phase diagram of the  $t$ - $J_s$ - $J_\tau$  model. Figure 3 shows the obtained phase diagram consisting of five phases: metallic phase (no excitation gap), spin-gap phase (only the spin gap opens), channel-gap phase (only the channel gap opens), insulating phase (gap opens for all excitations), and phase separation. From the diagram, it is confirmed that the spin-gap phase is realized in the TCKLM between the metallic and insulating phases.

As shown in Fig. 3, the transition lines are symmetric with respect to the line of  $J_s = J_\tau$ . This arises from the invariance of the Hamiltonian of Eq. (1) and the particle filling  $n = 1/2$  under the transformation  $(a_{i\uparrow}^\dagger, a_{i\downarrow}^\dagger, b_{i1}^\dagger, b_{i2}^\dagger) \rightarrow (b_{i1}^\dagger, b_{i2}^\dagger, a_{i\uparrow}^\dagger, a_{i\downarrow}^\dagger)$  with the exchange of  $J_s$  and  $J_\tau$ , where the symmetry of the repulsive term  $V$  is ensured by the condition of Eq. (2) [12]. Since this transformation exchanges the role of spin and channel degrees of freedom, the symmetric phase diagram is obtained. In the parameter sets we have studied, the direct transition between the metallic phase and the insulating phase occurs only on the line of  $J_s = J_\tau$ . This implies the existence of a quantum tetracritical point.

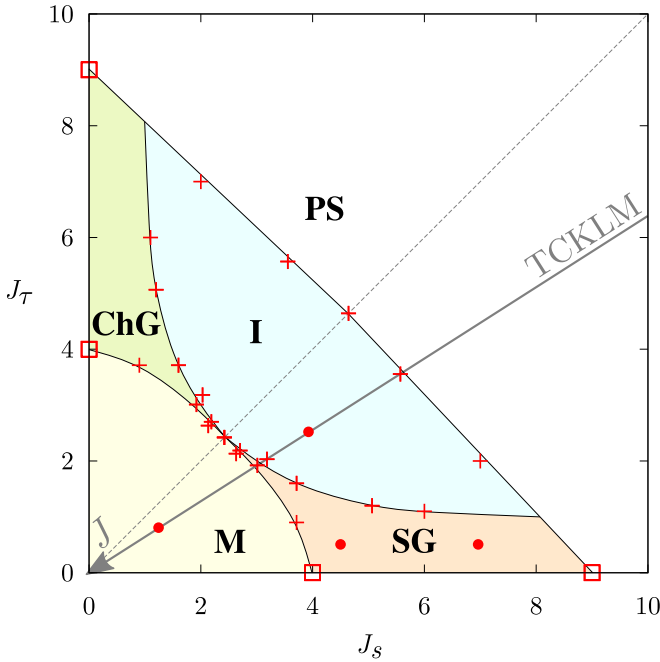


FIG. 3. Ground-state phase diagram of the  $t$ - $J_s$ - $J_\tau$  model. The plus marks represent the transition points. The phase boundary is roughly drawn. The squares on the transition line were determined in a previous work [3] for the extended  $t$ - $J$  model. The circles in the phase diagram represent the points where the correlation functions shown in Figs. 4, 6, and 7 are calculated. M, metallic phase (no excitation gap); SG, spin-gap phase (only the spin gap opens); ChG, channel-gap phase (only the channel gap opens); I, insulating phase (gap opens for all excitations); and PS, phase separation.

### A. Metallic phase

Here we focus on the metallic phase in the region of weak interaction, where all the excitations are gapless and each spin, charge, and channel degree of freedom behaves as a Tomonaga-Luttinger liquid (TLL) [13,14]. As shown in Fig. 4,

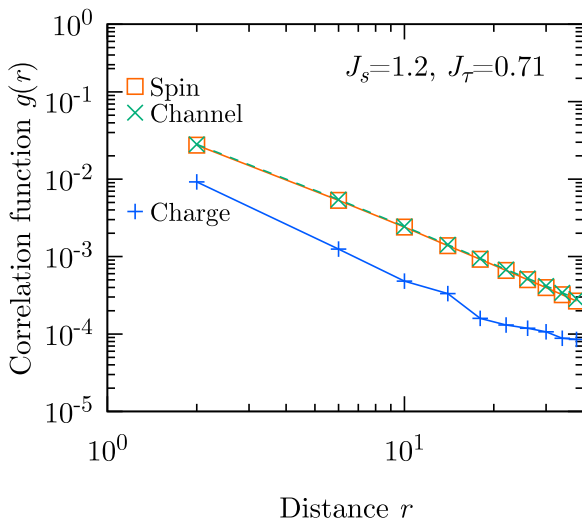


FIG. 4. Correlation functions in the metallic phase at  $J_s = 1.2$  and  $J_\tau = 0.71$  ( $J = 9.0$ ).

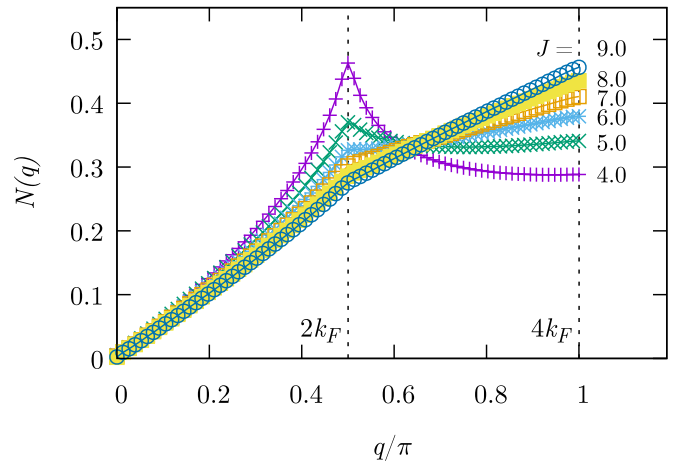


FIG. 5. Fourier components of the charge correlation function. Central  $L = 152$  sites of a 192-site system are used to suppress the boundary effects. The dominant wavelength changes from  $4k_F$  to  $2k_F$  with the decrease in  $J$  (with the increase in  $J_s$  and  $J_\tau$ ).

the correlation functions defined by

$$g(r) = \langle X_j X_{j+r} \rangle - \langle X_j \rangle \langle X_{j+r} \rangle, \quad (6)$$

$$X_j = \begin{cases} n_j & \text{(for charge),} \\ S_j^z & \text{(for spin),} \\ \tau_j^z & \text{(for channel)} \end{cases} \quad (7)$$

decay in a power-law fashion  $r^{-\alpha}$ . For spin and channel degrees of freedom, the exponent is  $\alpha \sim 1.6$  at  $J = 9$ , which is almost consistent with the prediction of TLL theory  $\alpha = 1 + K_\rho$ , where the Luttinger parameter  $K_\rho$  is determined as  $K_\rho \sim 0.5$  from the slope of the Fourier components of the charge correlation function  $N(q)$  near  $q = 0$  [2,15,16]. The  $J_s$  dependence of  $N(q)$  defined by

$$N(q) = \frac{1}{L} \sum_{i,j=1}^L e^{iq(x_i - x_j)} (\langle n_i n_j \rangle - \langle n_i \rangle \langle n_j \rangle) \quad (8)$$

also shows that the period of the charge correlation function clearly changes from  $4k_F$  (two site) to  $2k_F$  (four site) with the increase in  $J_s$  and  $J_\tau$  as presented in Fig. 5.

When  $J_s$  exceeds a critical value, the system undergoes the transition to the spin-gap phase. At  $J_\tau = 0$ , the critical value of  $J_s$  is close to the bandwidth  $4t$ . Figure 3 shows that this critical value becomes smaller with the increases in  $J_\tau$ , which indicates the interaction acting on the channel degree of freedom stabilizes the spin-gap phase. We note that the critical value is insensitive to  $V$  when  $V$  is sufficiently smaller than  $4t$ .

### B. Spin-gap phase

As discussed above, the increase in  $J_s$  and  $J_\tau$  enhances the spin gap, which makes the slope of the exponential decay of the spin correlation function steeper, as shown in Fig. 6(a). For the charge and channel correlation functions, the power-law behavior is confirmed, as seen in Fig. 6(b). The power-law exponent of the charge correlation function slightly decreases with the increase in the spin gap.

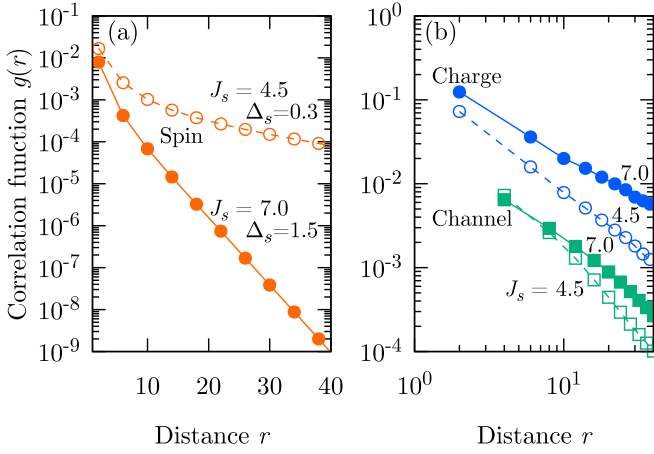


FIG. 6. Correlation functions in the spin-gap phase at  $J_\tau = 0.5$ . (a) Spin correlation function. (b) Charge and channel correlation functions.

### C. Insulating phase

We finally investigate the insulating state. In the insulating phase, all the excitations have a finite energy gap, and the correlation functions decay exponentially, as shown in Fig. 7, where we find almost the same slope, although the charge gap is much smaller than the spin gap. We think this is a result of the alternating product state wave function of the spin and channel singlets, as shown later.

To find the symmetry-breaking order of the insulating phase, we calculate several local expectation values. Figure 8 shows the site dependence of the local densities and nearest-neighbor correlations, defined as

$$f_s(i) = \langle S_{i-1/2}^z S_{i+1/2}^z \rangle - \langle S_{i-1/2}^z \rangle \langle S_{i+1/2}^z \rangle, \quad (9)$$

$$f_\tau(i) = \langle \tau_{i-1/2}^z \tau_{i+1/2}^z \rangle - \langle \tau_{i-1/2}^z \rangle \langle \tau_{i+1/2}^z \rangle, \quad (10)$$

where  $i$  is the center position of the two operators. We find the charge density  $\langle n_i \rangle$  has  $2k_F$  (four-site) oscillation, whereas the

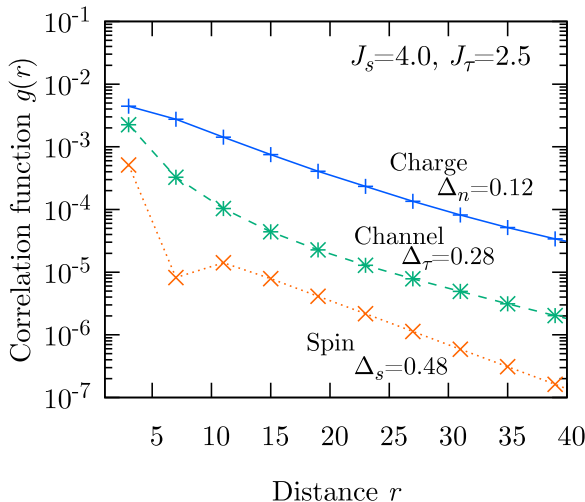


FIG. 7. Correlation functions in the insulating phase at  $J_s = 4.0$  and  $J_\tau = 2.5$ .

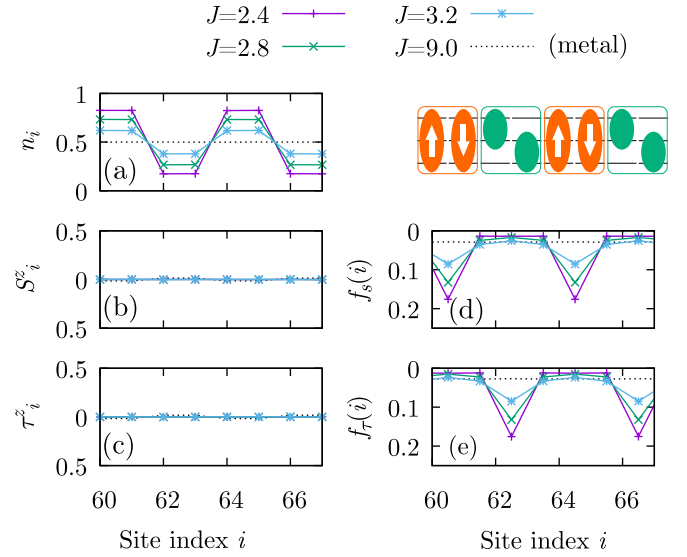


FIG. 8. Site-dependent expectation values in the insulating phase at  $J = 2.4, 2.8,$  and  $3.2$ . (a), (b), and (c) represent local densities. (d) and (e) show the nearest-neighbor correlations. The dotted line shows those in the metallic phase at  $J = 9.0$  for comparison. The top right diagram shows a schematic picture of the ground state. The rounded rectangles represent singlet pairs.

spin and channel densities  $\langle S_i^z \rangle$  and  $\langle \tau_i^z \rangle$  remain zero everywhere. In addition, the nearest-neighbor correlations strongly correlate with the charge density oscillation. These results suggest that the insulating phase is a product state of spin and channel singlets, as schematically shown in Fig. 8. The spin-gap state is then considered as a state in which only the spin degree of freedom forms singlet pairs.

As shown in Fig. 3, the transition to the insulating state and the opening of the channel gap simultaneously occur in the region of  $J_s > J_\tau$ . With the increase in  $J_s$  from zero, the critical value of  $J_\tau$  which opens the channel gap decreases from almost the bandwidth of  $4t$  to  $t$  but never goes down to zero, which indicates the cooperation of the spin and channel degrees of freedom is essential for the emergence of the insulating phase.

Here we comment on the effect of the nearest-neighbor repulsion  $V$ . This term is added to effectively include the higher-order interactions existing in the original TCKLM, which suppress the transition to the phase separation. As the nearest-neighbor repulsion leads to the metal-insulator transition in the extended Hubbard model at quarter filling [17,18], this may affect the phase diagram. However, the insulating state caused by the nearest-neighbor repulsion  $V$  is characterized by the  $4k_F$  (two sites) charge densities, which is clearly different from the insulating state found in the present study, where only  $2k_F$  (four sites) oscillation appears. We therefore think the repulsion term is not essential in the present analysis.

### V. CONCLUSION

We have studied the ground states of the  $t$ - $J_s$ - $J_\tau$  model, which is a minimal model consisting of multiple degrees

of freedom. The low-energy excitations of the spin, charge, and channel degrees of freedom have been calculated by the DMRG method with the SSD, and it was shown that the phase transition occurs from the metallic state to the spin-gap or channel-gap state when the exchange interactions exceed almost the bandwidth, roughly  $\sqrt{J_s^2 + J_t^2} \sim 4t$ . For the symmetric case of  $J_s = J_t$ , however, the direct transition to the insulating state takes place. These results imply that weak channel fluctuations stabilize the spin-gap state of the  $t$ - $J$

model, while strong channel fluctuations lead to the transition to the insulating state which is characterized by the alternating product state of the spin and channel singlets.

#### ACKNOWLEDGMENT

This work was supported by JSPS KAKENHI Grant No. JP19K03708.

- 
- [1] F. C. Zhang and T. M. Rice, *Phys. Rev. B* **37**, 3759 (1988).
  - [2] A. Moreno, A. Muramatsu, and S. R. Manmana, *Phys. Rev. B* **83**, 205113 (2011).
  - [3] M. Troyer, H. Tsunetsugu, T. M. Rice, J. Riera, and E. Dagotto, *Phys. Rev. B* **48**, 4002 (1993).
  - [4] D. L. Cox, *Phys. Rev. Lett.* **59**, 1240 (1987).
  - [5] T. Onimaru and H. Kusunose, *J. Phys. Soc. Jpn.* **85**, 082002 (2016).
  - [6] P. Nozières and A. Blandin, *J. Phys. (Paris)* **41**, 193 (1980).
  - [7] T. Schauerte, D. L. Cox, R. M. Noack, P. G. J. van Dongen, and C. D. Batista, *Phys. Rev. Lett.* **94**, 147201 (2005).
  - [8] S. R. White, *Phys. Rev. Lett.* **69**, 2863 (1992).
  - [9] S. R. White, *Phys. Rev. B* **48**, 10345 (1993).
  - [10] A. Gendiar, R. Krčmar, and T. Nishino, *Prog. Theor. Phys.* **122**, 953 (2009); **123**, 393 (2010).
  - [11] C. Hotta and N. Shibata, *Phys. Rev. B* **86**, 041108(R) (2012).
  - [12] In the system under the open boundary condition, the repulsive term modifies the local chemical potential at both ends of the system. In this study, we use the SSD and remove such a chemical-potential difference.
  - [13] F. D. M. Haldane, *J. Phys. C* **14**, 2585 (1981).
  - [14] J. Voit, *Rep. Prog. Phys.* **58**, 977 (1995).
  - [15] R. T. Clay, A. W. Sandvik, and D. K. Campbell, *Phys. Rev. B* **59**, 4665 (1999).
  - [16] H. J. Schulz, *Phys. Rev. Lett.* **64**, 2831 (1990).
  - [17] F. Mila and X. Zotos, *Europhys. Lett.* **24**, 133 (1993).
  - [18] T. Shirakawa and E. Jeckelmann, *Phys. Rev. B* **79**, 195121 (2009).